Nanoscale

PAPER

View Article Online
View Journal | View Issue

Cite this: *Nanoscale*, 2014, **6**, 2316

Spontaneous formation of light-trapping nano-structures for top-illumination organic solar cells†

Zheng-Yu Huang,[a] Si-Wen Chiu,[a] Chang-Wen Chen,[a] Yi-Hong Chen,[a] Li-Yen Lin,[b] Ken-Tsung Wong[bc] and Hao-Wu Lin*[a]

Received 24th October 2013
Accepted 2nd December 2013

DOI: 10.1039/c3nr05674k

www.rsc.org/nanoscale

By introduction of nano-structured crystallite capping layers, the power conversion efficiency of top-illumination organic solar cells is improved from 4.2 ± 0.1% to 6.0 ± 0.2%, representing a 44% enhancement. This is caused by the increase in J_{SC} and led by the enhancement in the local E distribution inside the active layers. Comprehensive finite-difference time domain simulation reveals two main reasons for this enhancement: (1) the nano-structured capping layers can be treated as gradient-index films that effectively increase the light entering the devices. (2) The nano-structured capping layers can also diffract the light from original normal-incident paths, hence increasing the absorption length inside the active layers.

Introduction

Organic solar cells (OSCs) have been under intensive investigation because of their potential in the mass production of cost-effective, large-scale and flexible solar energy conversion devices.[1–4] Owing to the short exciton diffusion length (~10 nm)[5,6] and low charge carrier mobilities (10^{-5} to 10^{-3} cm^2 V^{-1} s^{-1}) of organic semiconductors,[7,8] a tradeoff and thus a bottleneck exists in the implementation of OSCs. Thicker active layers are preferred for efficient light harvesting, whereas thinner layers are desired for successful exciton dissociation and carrier collection. To overcome this difficulty, tremendous effort in material design, processing techniques and device architecture has been made steadily to increase the power conversion efficiencies (PCEs) of OSCs.[9,10] In addition to the molecular and device engineering of active materials, manipulating the light in-coupling to improve the absorption efficiency of photoactive thin films is also one of the most promising methods for further enhancing the OSC efficiency.[4,11–17]

In our previous work, top-illuminated OSCs with microcavity structures were simulated and fabricated.[4] The potential of achieving high efficiency has been demonstrated by utilizing a suitable capping layer to reduce the high reflection caused by Ag thin films. The enhancement in the efficiency of the single quarter-wavelength capping layer, however, is restricted by a small wavelength range and narrow angles of incidence.[18] To extend the effective wavelength range and incident illumination angles, multi-layer or gradient-index coatings, which are used as anti-reflective coatings in lenses, can be employed.[19] In addition to applying one-dimensional layered structures, film surfaces can be textured with three-dimensional pyramids or two-dimensional grooves to effectively increase the in-coupling efficiency of solar cells.[20–25] However, the structures described above require complicated manufacturing processes and high fabrication costs.

In this paper, an alternative cost-effective method is presented. We exploited the properties of low-glass-transition-temperature organic materials to achieve nano-structured crystallite capping layers. The crystallite capping layers self-assembled into two- or three-dimensional nano-structures, which play similar roles to those of grooves or pyramids in anti-reflective textured surfaces. With the use of OptiFDTD (Optiwave Systems Inc.), the optical effects of crystallite capping layers were investigated. The application of crystallite capping layers can dramatically decrease the reflection of microcavity devices and enhance their efficiency by 44%, from 4.2 ± 0.1% to 6.0 ± 0.2%.

Results and discussion

The effects of the capping layers are highly affected by the ratio of their dimensions to the wavelength of incident light: (1) if a nano-structure is much smaller than the interaction wavelength, the so-called long wavelength limit, the surface region will behave as a gradient-index film, and its optical properties can be described by the effective medium theory.[26,27] (2) If a surface structure's size is much greater than the interaction wavelength, in other words, if the structure is in the short

[a]*Department of Materials Science and Engineering, National Tsing Hua University, No. 101, Section 2, Kuang-Fu Road, Hsinchu, 30013, Taiwan. E-mail: hwlin@mx.nthu.edu.tw*

[b]*Department of Chemistry, National Taiwan University, Taipei, 10617, Taiwan*

[c]*Institute of Atomic and Molecular Sciences, Academia Sinica, No. 1, Section 4, Roosevelt Road, Taipei, 10617, Taiwan*

† Electronic supplementary information (ESI) available. See DOI: 10.1039/c3nr05674k

wavelength limit, ray optics will be needed to explain how rays would be reflected multiple times before being sent back toward the source.[28] (3) If the physical size of a nano-structure is comparable with the wavelength range of visible light, interference effects must be considered. Hence, in this case, the effective medium theory and ray optics calculations are not adequate for an accurate simulation.[20]

Bphen (4,7-diphenyl-1,10-phenanthroline) and NTCDA (naphthalenetetracarboxylic) were selected as nano-structured capping layers owing to their tendency to crystallize at room temperature.[29–31] Devices were fabricated with a thick silver film (120 nm) deposited onto a glass substrate as the anode. MoO_3 (20 nm), as the hole-transporting layer, was deposited onto the anode, followed by the deposition of a donor neat film composed of DTDCTP (2-{[2-(5-*N*,*N*-di(*p*-tolyl)aminothiophen-2-yl)-pyrimidin-5-yl]methylene}malononitrile, 7 nm), a mixed layer of DTDCTP and C_{70} (1 : 1, by volume, 40 nm), an acceptor neat film composed of C_{70} (7 nm), an electron-transporting layer composed of BCP (2,9-dimethyl-4,7-diphenyl-1,10-phenanthroline, 10 nm) and a thin silver film (12.5 nm) as the cathode. Finally, a capping layer composed of Bphen or NTCDA (40 nm) was deposited onto the device. The devices were then encapsulated in a glove box. The encapsulated devices were held at room temperature for ~24 hours to fully develop the Bphen or NTCDA nano-structures. It should be noted that the nano-structures were automatically self-assembled without any treatment and the morphology was fixed after the development of the nano-structures. The final device structure with an organic crystallite capping layer is shown schematically in the inset of Fig. 1.

Fig. 1 shows the current density–voltage (*J*–*V*) curves of the devices with and without the organic nano-structured capping layers. Compared with the reference cell without the nano-structured capping layers, it can be easily observed that there was a dramatic increase in the short-circuit current densities (J_{SC}) of the cells with capping layers. The J_{SC} values of the devices with a Bphen capping layer and an NTCDA capping layer were 12.1 (11.8 ± 0.3) and 11.3 (11.1 ± 0.2) mA cm^{-2}, respectively, whereas the reference cell showed a J_{SC} value of merely 9.4 (9.2 ± 0.2) mA cm^{-2}. Because the capping layer outside the cathode was the only difference between these cells, the increase in current density, which can also be observed in the external quantum efficiency (EQE) spectra shown in Fig. 2, was most likely caused by optical effects rather than improvements in the electronic properties of the devices. Among these devices, the one with the Bphen capping layer exhibited the best performance, demonstrating an open-circuit voltage of 0.94 ± 0.02 V, a fill factor of 0.53 ± 0.01 and an overall power conversion efficiency (PCE) of 6.0 ± 0.2%, with the highest PCE of up to 6.2%. This device showed an efficiency 44% higher than that of the reference cell (PCE = 4.2 ± 0.1%).

The EQE spectra indicate that the devices with capping layers showed superior performance compared with the reference cell over the entire wavelength range, with the exception that the EQE was lower for the NTCDA-capped device at wavelengths below 420 nm. The lower EQE of the NTCDA-capped device at short wavelengths is attributed to the ultra-violet to violet absorption of NTCDA, whereas the different degrees of enhancement in EQE are due to the different degrees of light in-coupling caused by the different refractive indices and surface morphologies of NTCDA and Bphen. To evaluate the effect of nano-structured crystallite organic capping layers on the performance of microcavity cells, reflection spectra were obtained (Fig. 2). With the help of an integrating sphere, the diffuse reflections caused by the irregular surface of the crystallite capping layers could be carefully considered. The reflection spectra show that the reflection of the device without a capping layer was indeed higher than that of the devices with capping layers across the entire range of wavelengths. The lower reflections of the NTCDA-capped and Bphen-capped devices indicate that the crystallite capping layers possess anti-reflective properties and thus act as efficient light in-coupling structures for OSCs.

To understand the mechanism underlying the decrease in reflection and enhancement of the device EQE, the surface morphologies of the nano-structured capping layers must be considered. To observe the surface morphology, atomic force microscopy (AFM) and scanning electron microscopy (SEM)

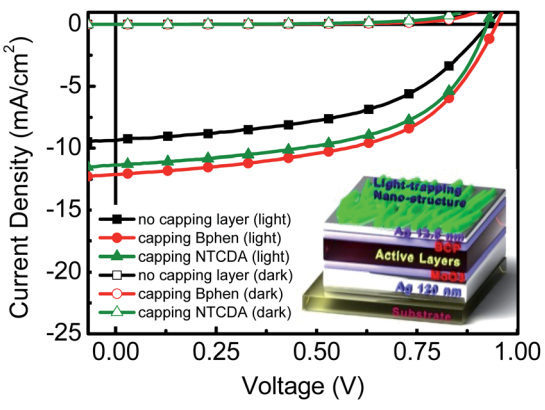

Fig. 1 Dark and illuminated (AM 1.5G, 1 sun) *J*–*V* curves of the top-illuminated devices with and without a nano-structured crystallite organic capping layer. Inset: illustration of top-illuminated microcavity device structure used in this study.

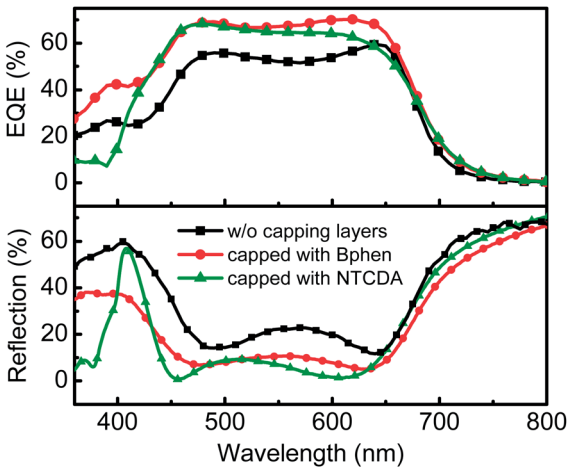

Fig. 2 EQE and reflection spectra of the top-illuminated devices with and without a nano-structured crystallite organic capping layer.

were applied. Fig. 3(a)–(c) show stereoscopic, tilted-view SEM images and AFM images of the devices without a capping layer with the Bphen capping layer and with the NTCDA capping layer, respectively. The surface morphology of the 12.5 nm thick silver film (without capping layer) is smooth with a root mean square roughness (R_q) as low as 1.1 nm, whereas the morphologies of the other two are much rougher. Strip-like structures can be observed in the Bphen layer with a R_q up to 22.4 nm, whereas granular structures can be observed in the NTCDA layer with a R_q of 5.8 nm. Because the physical sizes of both the Bphen and NTCDA nano-structures are comparable at visible light wavelengths, the finite-difference time domain (FDTD) method was selected as the simulation tool. The FDTD method calculates the numerical solution to Maxwell's equations directly and is valid for all structure dimensions (much greater than, much less than and approximately equal to the wavelength range of visible light).[32]

The simulations were simplified to two-dimensional cases, and both transverse electric (TE) and transverse magnetic (TM) modes were considered. All optical constants (wavelength dependent refractive index, n, and extinction coefficient, k) used in the models were carefully obtained using a spectroscopic ellipsometer, and the surface structures of the capping layers used in the different geometries were extracted from the profiles of the AFM images. The X–Z plane is the plane of incidence, and plane waves propagate in the Z-direction. The propagation of continuous, plane electromagnetic (EM) waves at wavelengths of 450 nm, 540 nm and 640 nm through structures with various capping layers was modeled. During the numerical calculation, the electric field (E) and the Poynting vector (S) at every location were recorded. After a sufficient number of time steps, the results converged to stable values. In addition to the FDTD method, we also utilized the transfer matrix method (TMM) to calculate the electric field in reference devices without capping layers.[33] It should be noted that the E distribution calculated by the TMM shows great consistency with the results obtained by the FDTD method, thus confirming that the final results obtained by the FDTD method approached the steady state (see Fig. S1 in the ESI†). Fig. 4 shows contour plots of the E distribution in devices with a Bphen capping layer at wavelengths of 450 nm and 640 nm. The device structure used in the simulation is also depicted in the figures. The E distribution at 540 nm and the E distribution of the NTCDA-capped devices are shown in Fig. S2 and S3 in the ESI.† It can be observed that the electric field distribution varies with the surface nano-structures of the capping layers, and the local enhancement of the electric field in the active layers can be observed.

To further investigate the effect of capping layers on the optical fields of the devices, we plotted $|E|^2$ along the

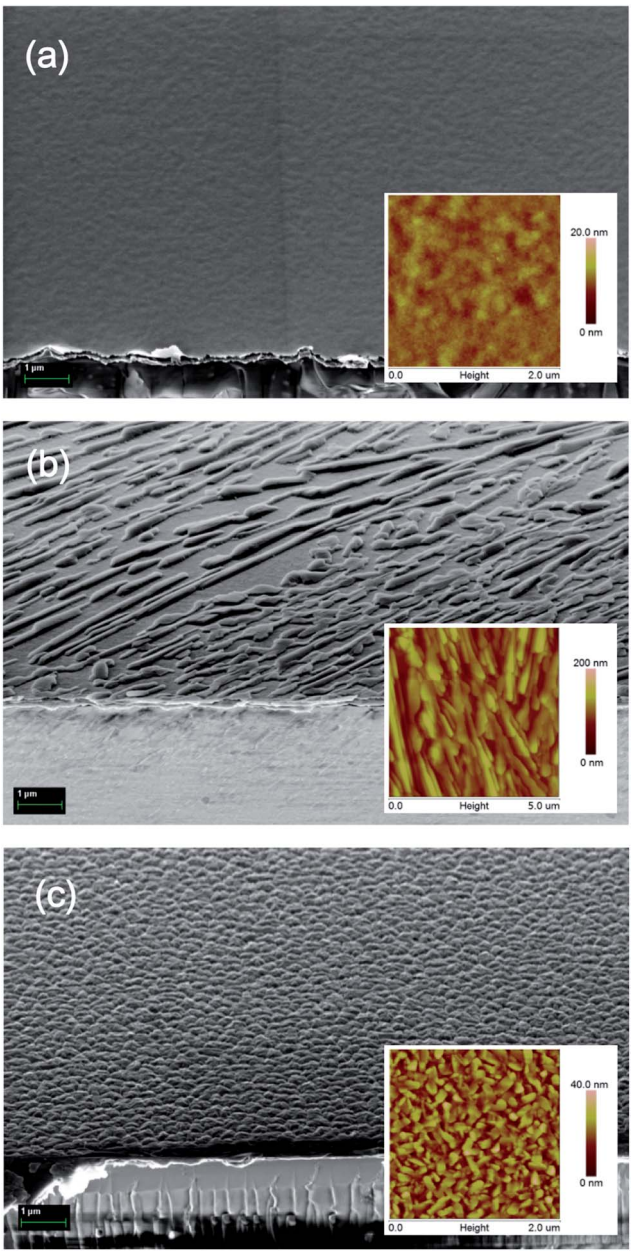

Fig. 3 SEM images of the devices (a) without capping layers, (b) capped with Bphen and (c) capped with NTCDA. Inset: AFM images of devices (a) without capping layers, (b) capped with Bphen and (c) capped with NTCDA.

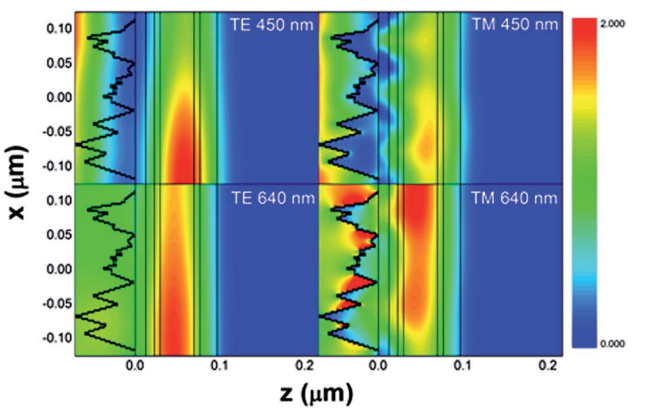

Fig. 4 E distribution in TE and TM polarization modes at wavelengths of 450 nm and 640 nm in the Bphen-capped device. The device structure used in the simulation is depicted by black lines. From left to right: air/Bphen/Ag/BCP/C_{70}/DTDCTP:C_{70}/DTDCTP/MoO_3/Ag.

X-direction at each *Z* position, as shown in Fig. 5. The figure clearly shows that the values of $|E|^2$ are higher in devices with capping layers than in the reference device, proving that the capping layers indeed increase the amount of light entering the active layers. The physics behind this phenomenon is typically explained by using the effective medium theory.[18] The volume ratios of Bphen or NTCDA to air increase monotonically from the air side to the device side. In other words, the relative fractions of the structure components become larger in the light-propagating direction. Light passing through the nano-structured region experiences a surrounding n that varies gradually from low ($n = 1$ in air) to high ($n \sim 1.7$ in Bphen or NTCDA neat film). Hence, the light passes through the capping layer region because there is no interface between air and the top electrodes ($n \sim 0.12$, $k = 2$–5 in Ag, wavelength dependent optical constants of Bphen, NTCDA and Ag: see Fig. S4 in the ESI†) of the devices. As a result, the capping layer acts as a good buffer to reduce the dielectric contrast between air and Ag and thus increases the amount of light that enters the devices. Because the n value of both Bphen and NTCDA is approximately 1.7, the layer with larger surface structures (the Bphen-based capping layer) creates a lower dielectric contrast. As shown in Fig. 3(b), the roughness of the Bphen capping layer is much higher than that of the NTCDA layer; therefore, the *E* distributions in Bphen-capped devices should be higher than those in NTCDA-capped devices. However, the electric field distributions show little difference between Bphen-capped and NTCDA-capped devices owing to the lower coverage ratio of Bphen capping layers, which can be easily observed in SEM images (Fig. 3). Therefore, an additional analysis of the *S* distribution inside the cells was performed to clarify the advantage of Bphen layers over NTCDA.

In addition to increasing the amount of light entering the devices, capping layers can also diffract transmitted light from the direction of incidence, inducing a lateral component in *S*, which can effectively increase the absorption path length in active materials.[34] Fig. 6 shows the ratios of the Poynting vectors in the *X*-direction (S_X) to the Poynting vectors in the *Z*-direction (S_Z) inside the active layers. The ratios are higher in devices with Bphen capping layers at all wavelengths due to the higher surface roughness. This result indicates that Bphen capping layers diffract incident light along the normal direction and increase the absorption pathway more efficiently than NTCDA capping layers.

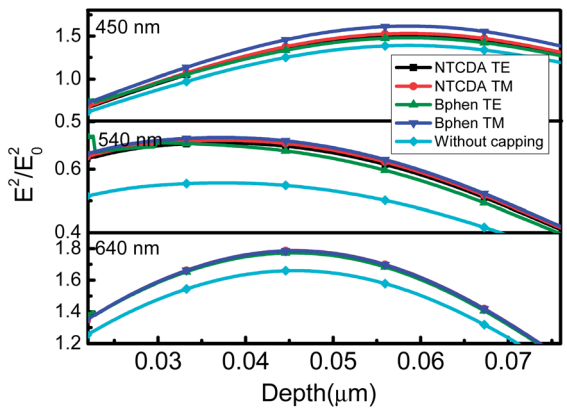

Fig. 5 The distribution of spatially averaged *E* along the *X*-direction inside the active layers at wavelengths of 450 nm, 540 nm and 640 nm.

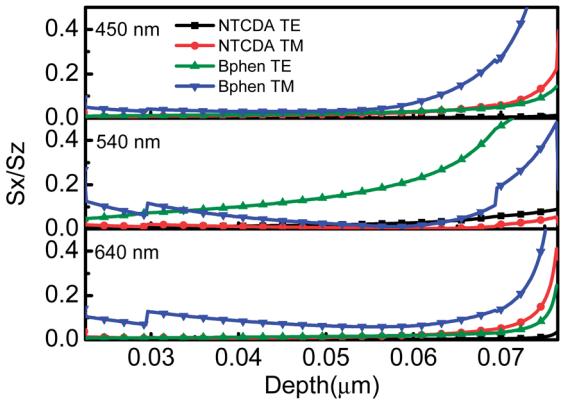

Fig. 6 Ratios of spatially averaged S_X and S_Z inside the active layers at wavelengths of 450 nm, 540 nm and 640 nm.

Conclusions

In conclusion, the performance of OSCs with microcavity structures was effectively enhanced by judiciously making use of organic nano-structured crystallite capping layers. The improvement in the efficiency from 4.2 ± 0.1% to 6.0 ± 0.2%, representing a 44% enhancement, was caused by the increase in J_{SC} and led by the enhancement in the local *E* distribution inside the active layers. Using FDTD simulation, two reasons for this enhancement were determined: (1) the capping layers can be treated as gradient-index films that effectively increase the amount of light entering the devices and (2) the capping layers can also diffract the light from original normal-incident paths, hence increasing the absorption length inside the active layers. We believe that the methodology of creating self-assembled nano-structures for light-trapping reported in this study can also be applied to general top-illuminated OSCs using either polymers or small molecules as solar absorbing materials and other inorganic-based devices. The calculation and experimental results also suggest that the efficiency could be further improved by using capping layers with larger surface structures and higher coverage ratios.

Experimental

Organic compounds, including synthesized DTDCTP, commercially obtained fullerene C_{70}, 2,9-dimethyl-4,7-diphenyl-1,10-phenanthroline (BCP), 4,7-diphenyl-1,10-phenanthroline (Bphen) and naphthalenetrtracarboxylic (NTCDA) were subjected to purification at least once by temperature-gradient sublimation before use in this study. The organic, metal oxide thin films, salts and metal electrodes were deposited on precleaned substrates in a high-vacuum chamber with a base pressure $\approx 1 \times 10^{-6}$ Torr. The deposition was performed at a rate of 1–2 Å with the substrate held at room temperature.

Film thicknesses were monitored using a crystal oscillator during deposition and were later verified by spectroscopic ellipsometry. The active area of the cells had an average size of 5 mm^2. The current density was measured using a Source Meter Keithley 2636A under AM 1.5G solar light emitted from a xenon lamp solar simulator (Abet Technologies). The incident light intensity was calibrated to be 100 mW cm^{-2} using a NREL-certified monocrystalline silicon reference cell with a KG-5 filter. The deviation values of cell performance were obtained from device-to-device variations of 4–8 devices. External quantum efficiency spectra were obtained by illuminating chopped monochromatic light with a continuous-wave white-light bias (from a halogen lamp) on the solar cells. Photocurrent signals were extracted by the lock-in technique using a current preamplifier (Stanford Research System) followed by a lock-in amplifier (AMETEK). The external quantum efficiency measurement was fully computer controlled, and the intensity of the monochromatic light was carefully calibrated with a NIST-traceable optical power meter (Ophir Optronics). Ellipsometry measurements were carried out with a J. A. Woollam Inc. V-VASE variable-angle spectroscopic ellipsometer. The simulation program used to implement the transfer matrix method was coded in the Matlab software program (The MathWorks, Inc.) and executed on a dual-core Intel-CPU personal computer. The FDTD simulation was performed using the OptiFDTD simulation program (Optiwave Systems Inc.). Absorption spectra were obtained using a spectrometer with an integrating sphere reflectance accessory (PerkinElmer).

Acknowledgements

The authors would like to acknowledge the financial support from the National Science Council of Taiwan (NSC-102-2221-E-007-125-MY3, NSC-101-2112-M-007-017-MY3 and NSC102-2633-M-007-002) and the Low Carbon Energy Research Center, National Tsing Hua University. The authors also appreciate the help with the SEM measurement by Professor Chih-Wei Chang.

Notes and references

1 W. Chen, M. P. Nikiforov and S. B. Darling, *Energy Environ. Sci.*, 2012, **5**, 8045.
2 D. Yue, P. Khatav, F. You and S. B. Darling, *Energy Environ. Sci.*, 2012, **5**, 9163.
3 S. B. Darling and F. You, *RSC Adv.*, 2013, **3**, 17633.
4 H. W. Lin, S. W. Chiu, L. Y. Lin, Z. Y. Hung, Y. H. Chen, F. Lin and K. T. Wong, *Adv. Mater.*, 2012, **24**, 2269.
5 D. R. Kozub, K. Vakhshouri, S. V. Kesava, C. Wang, A. Hexemer and E. D. Gomez, *Chem. Commun.*, 2012, **48**, 5859.
6 Y. Terao, H. Sasabe and C. Adachi, *Appl. Phys. Lett.*, 2007, **90**, 103515.
7 M. M. Mandoc, L. J. A. Koster and P. W. M. Blom, *Appl. Phys. Lett.*, 2007, **90**, 133504.
8 G. Garcia-Belmonte, A. Munar, E. M. Barea, J. Bisquert, I. Ugarte and R. Pacios, *Org. Electron.*, 2008, **9**, 847.
9 R. Fitzner, E. Mena-Osteritz, A. Mishra, G. Schulz, E. Reinold, M. Weil, C. Korner, H. Ziehlke, C. Elschner, K. Leo, M. Riede, M. Pfeiffer, C. Uhrich and P. Bauerle, *J. Am. Chem. Soc.*, 2012, **134**, 11064.
10 A. K. Kyaw, D. H. Wang, V. Gupta, W. L. Leong, L. Ke, G. C. Bazan and A. J. Heeger, *ACS Nano*, 2013, **7**, 4569.
11 M. G. Kang, T. Xu, H. J. Park, X. Luo and L. J. Guo, *Adv. Mater.*, 2010, **22**, 4378.
12 S. Kim, J. F. Zhu, H. J. Shen, M. Xue, K. L. Wang, Z. B. Yu, L. Li, J. Park, Q. B. Pei and G. Park,*OSA/CLEO 2011, CMCC1,* 2011.
13 K. Q. Le, A. Abass, B. Maes, P. Bienstman and A. Alù, *Opt. Express*, 2011, **20**, A39.
14 M. A. Sefunc, A. K. Okyay and H. V. Demir, *Opt. Express*, 2011, **19**, 14200.
15 Y. Long, *Appl. Phys. Lett.*, 2009, **95**, 193301.
16 J. L. Wu, F. C. Chen, Y. S. Hsiao, F. C. Chien, P. L. Chen, C. H. Kuo, M. H. Huang and C. S. Hsu, *ACS Nano*, 2011, **5**, 959.
17 H.-Y. Wei, J.-H. Huang, C.-Y. Hsu, F.-C. Chang, K.-C. Ho and C.-W. Chu, *Energy Environ. Sci.*, 2013, **6**, 1192.
18 I. Powell, *Principles of Optics*, Taylor & Francis, 1976.
19 H. A. Macleod, *Thin-Film Optical Filters*, Taylor & Francis, 4th edn, 2010.
20 A. Deinega, I. Valuev, B. Potapkin and Y. Lozovik, *J. Opt. Soc. Am. A*, 2011, **28**, 770.
21 P. B. Clapham and M. C. Hutley, *Nature*, 1973, **244**, 281.
22 K. Sahoo, M. K. Lin, E. Y. Chang, Y. Y. Lu, C. C. Chen, J. H. Huang and C. W. Chang, *Nanoscale Res. Lett.*, 2009, **4**, 680.
23 Y. F. Huang, S. Chattopadhyay, Y. J. Jen, C. Y. Peng, T. A. Liu, Y. K. Hsu, C. L. Pan, H. C. Lo, C. H. Hsu, Y. H. Chang, C. S. Lee, K. H. Chen and L. C. Chen, *Nat. Nanotechnol.*, 2007, **2**, 770.
24 Y. M. Song, S. Y. Bae, J. S. Yu and Y. T. Lee, *Opt. Lett.*, 2009, **34**, 1702.
25 C. Cho, H. Kim, S. Jeong, S.-W. Baek, J.-W. Seo, D. Han, K. Kim, Y. Park, S. Yoo and J.-Y. Lee, *Sol. Energy Mater. Sol. Cells*, 2013, **115**, 36.
26 W. H. Southwell, *J. Opt. Soc. Am. A*, 1991, **8**, 549.
27 D. H. Raguin and G. M. Morris, *Appl. Opt.*, 1993, **32**, 2582.
28 B. L. Sopori and R. A. Pryor, *Sol. Cells*, 1983, **8**, 249.
29 B. W. D'Andrade, S. R. Forrest and A. B. Chwang, *Appl. Phys. Lett.*, 2003, **83**, 3858.
30 M. H. N. Hiroaki, JFE Technical Report, 2005, vol. 8, p. 8.
31 J.-H. Lee, M.-H. Wu, C.-C. Chao, H.-L. Chen and M.-K. Leung, *Chem. Phys. Lett.*, 2005, **416**, 234.
32 Y. Kane, *IEEE Trans. Antennas Propag.*, 1966, **14**, 302.
33 L. A. A. Pettersson, L. S. Roman and O. Inganäs, *J. Appl. Phys.*, 1999, **86**, 487.
34 P. Campbell and M. A. Green, *J. Appl. Phys.*, 1987, **62**, 243.

